Concept and Operation of a Wind Turbine Driven by Dynamic Stall

Keisar, David; De Troyer, Tim; Greenblatt, David

Published in:
AIAA Journal

DOI:
10.2514/1.J059487

Publication date:
2020

License:
Unspecified

Document Version:
Accepted author manuscript

Concept and Operation of a Wind Turbine Driven by Dynamic Stall

Journal:	*AIAA Journal*
Manuscript ID	Draft
Manuscript Type:	Express Article
Date Submitted by the Author:	n/a
Complete List of Authors:	Keisar, David; Technion, GTEP de Troyer, Tim; Vrije Universiteit Brussel, ; Greenblatt, David; Technion,
Subject Index Category:	00100 Aerodynamics < 00000 AIRCRAFT TECHNOLOGY, CONVENTIONAL, STOL/VTOL
Select ONE Subject Index for the Table of Contents. This is where your paper will show up in the Table of Contents:	10000 ENERGY

Concept and Operation of a Wind Turbine Driven by Dynamic Stall

David Keisar[1]
Technion – Israel Institute of Technology, Technion City, Haifa 3200003, Israel

Tim De Troyer [2]
Vrije Universiteit Brussel, Pleinlaan 2, 1050 Brussels, Belgium

and
David Greenblatt[3]
Technion – Israel Institute of Technology, Technion City, Haifa 3200003, Israel

Dynamic stall is exploited to produce positive torque on a large chord-radius ratio (*c*/*R*) vertical axis wind turbine (VAWT). An elementary kinematic analysis shows that the blades experience large variations in angle-of-attack that produce deep dynamic stall, combined with large relative dynamic pressure variations, that are phase-shifted by approximately 90°. The phase-shift allows dynamic lift overshoot effects associated with the formation of a dynamic stall vortex to drive the turbine when the relative dynamic pressure is high, while lift-stall associated with shedding of the vortex occurs when the relative dynamic pressure is low. Blades also experience variable virtual camber (or "virtual morphing") effects and favorable chordwise pressure gradients, where the former produces a virtual leading-edge droop that reduces the leading-edge angle-of-attack. Open jet wind tunnel tests of a two-bladed model turbine reveal maximum power coefficients of 16% that were almost independent of *c*/*R*. Flow visualization confirms that dynamic stall, with the associated dynamic stall vortex, is the mechanism that drives the turbine to maximum power. Due to the lack of reliable design tools for these machines, either empiricism and dimensional analysis or high-fidelity CFD are proposed for optimization and analysis.

[1] PhD Student, Grand Technion Energy Program, Faculty of Mechanical Engineering, AIAA Student Member.
[2] Assistant Professor, Faculty of Engineering, AIAA Member.
[3] Professor, Faculty of Mechanical Engineering; davidg@technion.ac.il. Associate Fellow AIAA.

Nomenclature

$\bar{a}$	=	average axial flow induction factor
c	=	blade mean chord-length
C_D	=	drag coefficient
C_L	=	lift coefficient
C_P	=	power coefficient
$(dz/dx)_{\text{eff}}$	=	effective (or virtual) camber
N	=	number of blades
R	=	turbine radius
Re	=	chord-based Reynolds number
q_{rel}	=	relative dynamic pressure
$\hat{q}_{\text{rel}}$	=	normalized relative dynamic pressure
U_i	=	local wind speed
U_∞	=	wind/free-stream speed
W	=	magnitude of the relative velocity
W^*	=	relative velocity magnitude along the chord
x	=	point along the chord
x_c	=	blade-strut connection point
α	=	angle-of-attack
$\dot{\alpha}$	=	blade pitch-rate
α^*	=	local angle-of-attack
α_s	=	static stall angle-of-attack
β	=	blade pre-pitch angle
β'	=	blade virtual pre-pitch angle
ε	=	chord-to-radius ratio
θ	=	turbine azimuthal angle

κ = blade dimensionless pitch-rate

λ = tip-speed ratio, $\Omega R / U_\infty$

ρ = air density

σ = turbine solidity

Ω = rotational speed

I. Introduction

In recent years, interest in vertical axis wind turbines (VAWTs) has surged [1]. Much of the research focusses on offshore applications [2] or urban-scale implementation [3] arising from well-known advantages such as insensitivity to the wind direction [4] and ground- or water-level location of the generator. Furthermore, symmetric and uniform blade profiles along the span can significantly reduce manufacturing costs. The performance range of VAWTs is strongly dependent on their solidity:

$$\sigma \triangleq Nc / R \tag{1}$$

where N is the number of blades, c is the blade mean chord-length and R is the turbine radius. In general, for high solidity machines $(\sigma > 0.4)$, the operational tip-speed ratios:

$$\lambda \triangleq \Omega R / U_\infty \tag{2}$$

where Ω is the rotational speed and U_∞ is the wind speed, are relatively low $(1 < \lambda < 2)$, while for low solidity turbines, they are relatively high $(3 < \lambda < 5)$ [5]. Although high solidity machines are less efficient, they have other important advantages for urban installations, such as lower noise emissions [6], lower probability of bird strikes [7] and better self-starting capabilities [8]. As a general rule, designers increase solidity by increasing the number of blades (N); it is far less common to increase the chord-length (c) to the point that the chord-length and radius have similar dimensions. In a break with convention, these turbines produce *useful positive torque as a result of dynamic stall*. The conceptual underpinnings, atypical aerodynamics and operation of these machines form the basis of this present paper.

The objectives of this paper are: (a) to describe the new concept of a dynamic stall driven turbine; and (b) to construct and test a small-scale demonstrator machine. Description of the operating principles and atypical aerodynamics of large blade-chord-to-radius ratio $(\varepsilon \triangleq c / R >> 0)$ turbines are presented in section II and wind tunnel

tests of the model are presented in section III. An elementary kinematic analysis serves as motivation for the approach adopted and illustrates the scope of the problem. The operational speeds of these high-solidity machines are typically low ($\lambda < 2$), which leads to so-called deep dynamic stall [9] in the presence of enormous variations in the relative dynamic pressure. This is accompanied by "virtual camber" (see [10] and section II. B) of the blades and chordwise pressure gradients. Although some of these factors have been recognized by other researchers [10][11], they have not been fully analyzed and the $\varepsilon >> 0$ regime has not been explored.

II. Large ε VAWT Kinematics

It is common knowledge that both the efficiency and structural integrity of low-solidity conventional VAWTs are adversely affected by dynamic stall [13], [14], which occurs when the blades pitch beyond their static stall angle-of-attack (α_s) [15]. The dynamic stall process begins with the appearance of reversed flow on the pressure surface, followed by the formation of a dynamic stall vortex (DSV) near the leading-edge that produces a static lift overshoot and then shedding of the DSV resulting in lift stall. In the analysis below, we shall consider a high-solidity, high chord-to-radius ratio design space where dynamic stall is exploited to drive the turbine.

A. Dynamic Stall to Produce Torque

For the purposes of our discussion, consider the simplified instantaneous velocity diagram at the center-span of an H-bladed VAWT shown in Fig. 1. We assume that power is only generated in the upwind quadrants of the azimuth ($0° \le \theta \le 180°$) and that the average axial flow induction factor $\bar{a} \equiv 1 - U_i / U_\infty$ is zero. From simple kinematics, the angle-of-attack at the strut-blade connection point is:

$$\alpha = \tan^{-1}\left(\frac{\sin\theta}{\lambda + \cos\theta}\right) \tag{3}$$

and the magnitude of the velocity relative to the blade is:

$$W = U_\infty \sqrt{(\lambda + \cos\theta)^2 + \sin^2\theta} \tag{4}$$

Thus the relative dynamic pressure is:

$$q_{\text{rel}} \equiv \tfrac{1}{2}\rho W^2 = \tfrac{1}{2}\rho U_\infty^2 \left[(\lambda + \cos\theta)^2 + \sin^2\theta\right] \tag{5}$$

which can be normalized as:

$$\hat{q}_{\text{rel}} \equiv (W / W_{\max})^2 \tag{6}$$

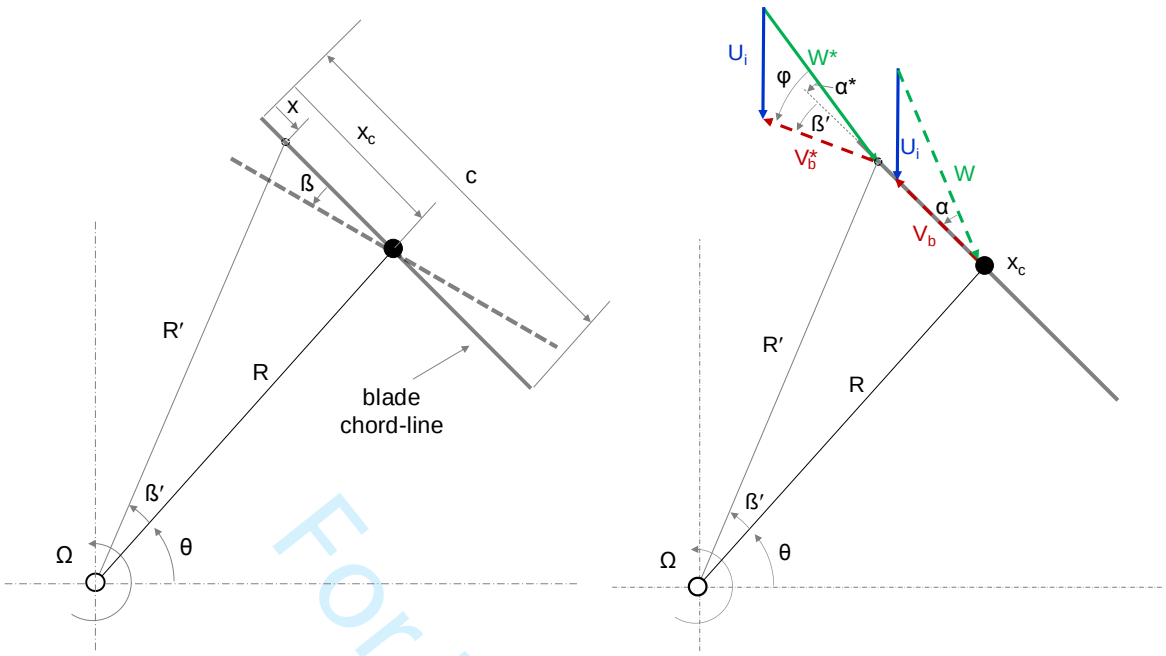

Fig. 1 Relevant dimensions (left) and simplified velocity kinematics (right) of a VAWT blade where $\varepsilon >> 0$

Curves for the nominal blade angle-of-attack α and normalized relative dynamic pressure $\hat{q}_{\text{rel}}$ as a function of azimuth θ are shown for λ=3 and 1.5 in Fig. 2a and Fig. 2b respectively. These results represent nominal values where the induction factor is zero and, by convention, $\varepsilon << 1$ is implicitly assumed [13]. In both cases, corresponding to slow rotation relative to the induced velocity though the rotor, moderate (λ=3) or large (λ=1.5) post-stall angles-of-attack are attained resulting in light or deep dynamic stall respectively [13]. On conventional turbines, the useful lift overshoot associated with the DSV formation is negated when it sheds from the blade, producing a sharp drop in the lift and an increase in drag. This results in a loss of torque and hence a power reduction in the stalled operation regime. It comes as no surprise that researchers aim to avoid dynamic stall by periodically pitching the blades [16] or attempt to control dynamic stall passively [17] or actively [18]-[21].

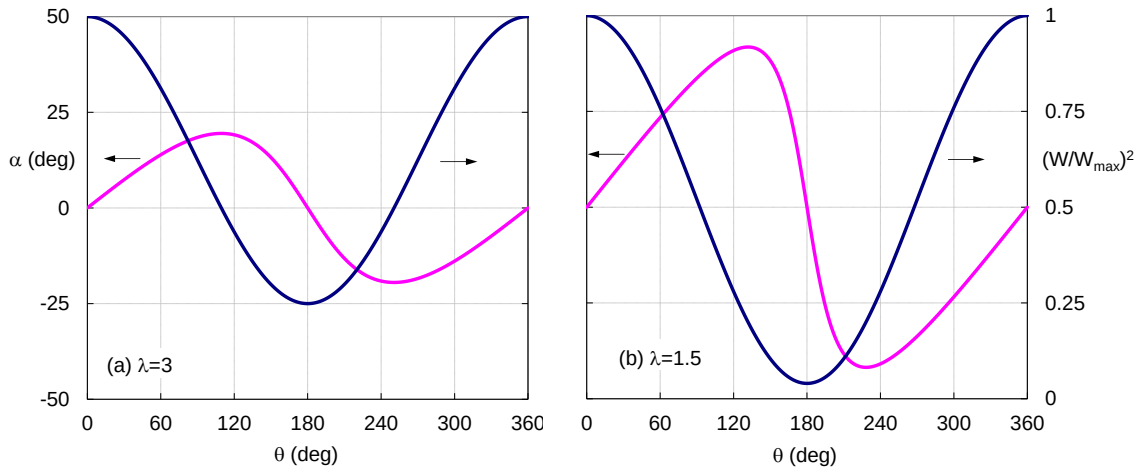

Fig. 2 Representative values of angle-of-attack (pink) and normalized relative dynamic pressure (blue) as a function of azimuthal angle for light and deep stall scenarios. Assumptions: induction factor equal to zero and ε<<1.

Fig. 2 also shows that relative dynamic pressure and angle-of-attack (based on the blade relative velocity magnitude) are out of phase by approximately 90°. This led us to consider a design space that exploits the positive lift-overshoot effects of dynamic stall to produce torque when q_{rel} is high, and mitigate the negative effects of the DSV shedding when q_{rel} is low. It is clear that conventional design techniques are of little use in this design space, and we must, therefore, resort to a combination of empiricism and dimensional analysis. In particular, a multitude of airfoil experiments indicate that static lift overshoot increases with increasing constant pitch rate $\kappa \triangleq \dot{\alpha}c/2U_\infty$ [13] or harmonic pitching frequency $k \triangleq \omega c/2U_\infty$ [15],[22]-[24]. On VAWTs, these definitions cannot be used because U_∞ must be replaced by W. Nevertheless, it can be shown that the blade pitch-rate is proportional to ε as suggested by Buchner *et al*. [25]. This confirms that, for a given design λ_d, the most effective way to increase the dimensionless pitch-rate, and hence the lift-overshoot, is to increase ε. This then serves as motivation for increasing the blade chord-length and not the number of blades in order to produce a high-solidity machine. The increase in chord-length produces higher blade Reynolds numbers, which is also an advantage, particularly for small machines whose blades suffer from low Reynolds number effects.

A VAWT blade is unique in that it pitches to positive and negative angles of attack and therefore usually undergoes dynamic stall twice in one cycle, upwind and downwind, where typically the dynamic stall timescale is some fraction of each half-cycle. Here, however, we assume that useful power is only generated in the upwind quadrants as was

demonstrated using blade surface pressure measurements [28]. Nevertheless, the timescales characterizing the dynamic stall process, from the development and shedding of the DSV to reattachment, are strongly dependent on the pitch-rate. Although the study of these timescales is beyond the purview of this paper, the timescale of the dynamic stall process for a $\varepsilon >> 0$ machine and that of the turbine rotation half-cycle should be comparable. More importantly, in instances where $\varepsilon >> 0$, the virtual camber of the blades and imposed pressure gradients cannot be considered to be fixed. This leads to unusual, or atypical, aerodynamics discussed in the next section.

B. Virtual Camber and Pressure Gradient

In instances where $\varepsilon >> 0$, the blade experiences significant variations in angle-of-attack and relative speed along its chord-length, as first explained by Migliore *et al*. [10]. This change in angle-of-attack can be modeled as a "virtual camber" combined with a superimposed pressure gradient and is explained with respect to Fig. 1. Here, we generalize the analysis of Migliore et al. [10] to account for the effect of the blade-strut connection point x_c, measured along the chord-line from the leading-edge, where the blade connects to the strut. Turbine blades may have an angle offset, known as the blade pre-pitch angle, β [11],[12]. In this analysis, without loss of generality, we assume β to be zero. Here we define a virtual pre-pitch angle between the rays emanating from the turbine axis to x_c (along R) and any arbitrary point x along the chord (along R'), namely:

$$\beta' = \sin^{-1}\left(\frac{x - x_c}{R'}\right) \tag{7}$$

which, for small angles, can be written in the form:

$$\beta' = (x^*/c)\varepsilon \tag{8}$$

where $x^* = x - x_c$. It is evident from Fig. 1 that the angle between the local blade velocity and local relative velocity varies as:

$$\varphi = \tan^{-1}\left(\frac{\sin(\theta + \beta')}{\lambda + \cos(\theta + \beta')}\right) \tag{9}$$

and hence from eqs. (8) and (9) we can express the local angle-of-attack as:

$$\alpha^* = \varphi - \beta' \tag{10}$$

and the chordwise change in angle-of-attack, or virtual camber, as:

$$(dz/dx)_{\text{eff}} = \alpha^* - \alpha \tag{11}$$

Likewise, the chordwise magnitude of the local relative velocity is:

$$W^* = U_\infty \sqrt{[\lambda + \cos(\theta + \beta')]^2 + \sin^2(\theta + \beta')} \tag{12}$$

and thus, the blade experiences an apparent chordwise acceleration, or pressure gradient equal to $(W^{*2} - W^2)/U_\infty^2$ after non-dimensionalizing.

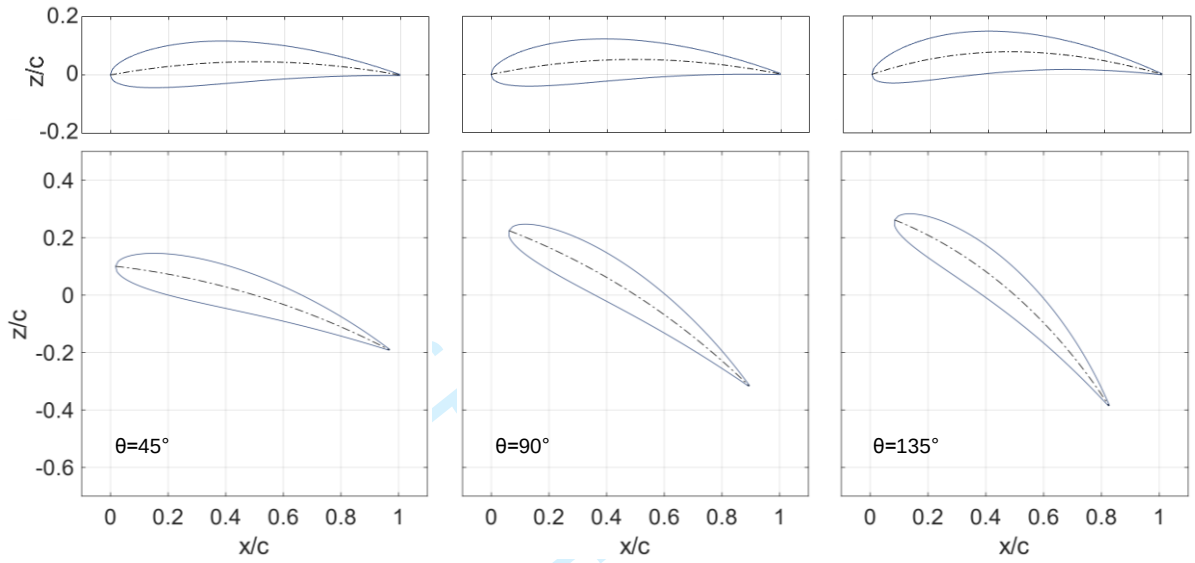

Fig. 3 NACA 0015 virtual camber line (top row) and blade orientation for horizontal relatively velocity (bottom row) at three azimuthal angles for $\varepsilon = 0.6$, $x_c/c = 0.5$ and $\lambda = 1.5$.

Fig. 3 shows the virtual camber lines and blade profile shapes of a NACA 0015 blade profile (top row) generated by integrating eq. (11) for $\varepsilon = 0.6$, $x_c/c = 0.5$ and $\lambda = 1.5$ together with blade orientation relative to a horizontal velocity vector (bottom row) from eq. (10). It can be seen that (in the upwind quadrants) the blade always experiences a virtual positive camber that increases with increasing θ. From $\theta = 45°$ to 135°, the virtual maximum camber increases from 4.5% to 7.7% (both at $x/c \approx 0.5$) and hence this process can be referred to as "virtual morphing". Virtual pitch-down of the leading-edge may serve to ameliorate dynamic stall (see below), while pitch-down of the trailing-edge may produce premature separation on the aft region of the blade. Although the strut connection point does not have a significant effect on the virtual camber-line (not shown), it does affect the local angle-of-attack. For example, $x_c/c = 0.25$ at $\theta = 90°$, results in 4.4% virtual camber (versus 4.7% for $x_c/c = 0.5$), but the local angle-of-attack at the leading-edge is 34° – 6° (versus 34° – 12° for $x_c/c = 0.5$). Another atypical aspect of $\varepsilon >> 0$ aerodynamics is that the blade is subjected to a favorable pressure gradient as illustrated in Fig. 4. This is roughly

equivalent to the aerodynamics of an airfoil in a converging channel. Although it is well known that favorable pressure gradients act to stabilize attached boundary layers, to the best of our knowledge no reliable aerodynamic load data exists for either static or dynamic airfoil performance under such conditions.

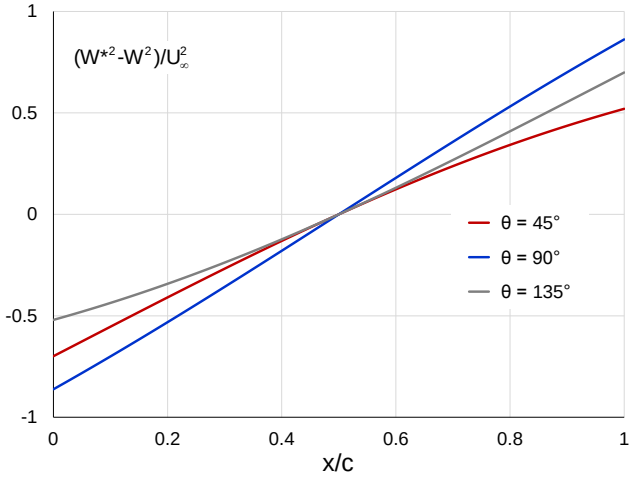

Fig. 4 Chordwise non-dimensional pressure gradients at three azimuthal angles for $\varepsilon = 0.6$, $x_c / c = 0.5$ and $\lambda = 1.5$. Similar results are obtained for $x_c / c = 0.25$.

III. Experimental Evaluation

A. Model Turbine and Wind Tunnel

To evaluate the hypothesis described above, a high ε VAWT was built and tested in a low-speed open jet wind tunnel. It employed an H-rotor configuration (Fig. 5, left) with two NACA 0015 blades of chord-length $c = 150\text{mm}$, connected to a vertical shaft (diameter $d = 50\text{mm}$), by means of variable-length horizontal struts of $R = 200,\ 300$ and 350mm. The shaft, bearing mounts and dynamometer system (Fig. 5) were similar to those used in previous investigations [18]-[21] and consisted of a Magtrol HB-140M2 hysteresis brake to regulate torque and a 1±0.0015 Nm Kistler 4502A1RAU torque meter (Fig. 5, right). The turbine was mounted in the center of a 1000 mm × 2000 mm test section. The brake was controlled via a TTi CPX400DP power supply with a control sensitivity of 0.001 A. This led to a 0.01-0.001 Nm torque control sensitivity. An optical sensor and a reflector located on the shaft were used to measure the turbine RPM with an estimated accuracy of ±2 RPM. All the sensors were connected to a LabVIEW analog-digital I/O and controlled through a dedicated program. The original tunnel nozzle [26] was removed and replaced by two inserts designed according to [27] to produce a 1600 mm × 2010 mm open jet. The average wind

tunnel speed ($U_\infty = 6.7 \pm 0.05$m/s for all experiments) was monitored by traversing a Pitot-static probe across the span of the test section at one diameter upstream of the turbine.

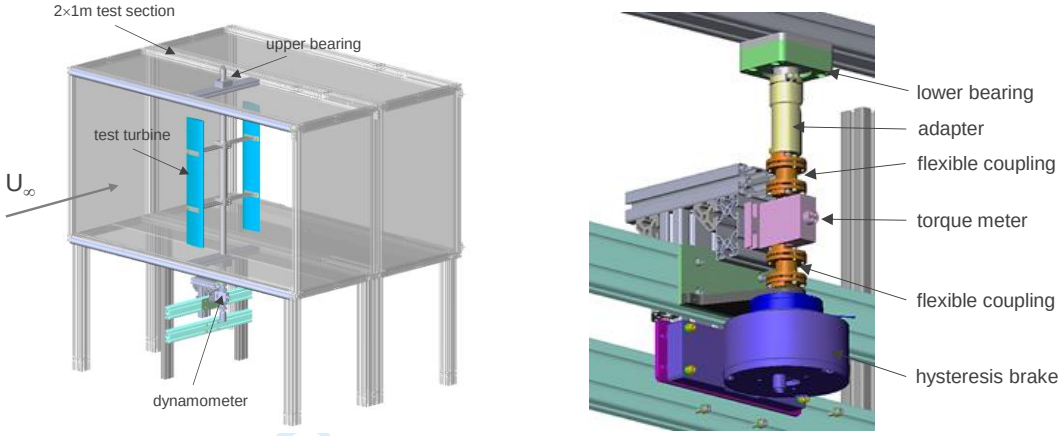

Fig. 5 Schematic of the turbine wind tunnel setup (left) and the dynamometer details (right).

Flow visualization was performed using 22mm-long, white fluorescent tufts attached inboard to a high contrast matte black paint covering 255mm of the blade span. The tufts were placed in the normal direction to the flow, pointing downwards. A total of 42 tufts on each blade were spaced using a 22mm × 40mm grid and attached to the surface using a 75 μm polyamide tape. A 180W UV diode cannon was used to illuminate the tufts, while a high-speed Phantom v7.3 camera, recording at 5000 frames per second, was used to videotape the tufts.

B. Experimental Results

Initial experiments were attempted with the strut connection point at $x_c / c = 0.25$ and $\varepsilon = 0.6$, but the turbine did not produce positive torque. Subsequently, the connection point was shifted aft to $x_c / c = 0.38$ and the turbine did indeed produce positive torque as shown in Fig. 6, attaining $C_{P,\max} \approx 10\%$. A further shift aft to $x_c / c = 0.5$ produced $C_{P,\max} \approx 16\%$, which is approximately half of the commercially-available best performing high-solidity VAWTs [11], although those turbines typically operate at higher Reynolds numbers. Unfortunately, the blade design did not facilitate further aft connection and thus additional experiments, at $\varepsilon = 0.5$ and 0.4, were conducted with $x_c / c = 0.5$ (Fig. 6). It is reasonable to assume, however, that moving the connection point further aft will produce even larger power coefficients. As expected, the λ for optimum power increased with decreasing ε together with a small increase in the operation range (the difference between maximum and minimum λ). In contrast to other studies [28], the

maximum power coefficient did not increase with decreasing solidity. This might be due to the fact that we decrease ε as opposed to reducing N to decrease the solidity. It is difficult to pin down to a single factor because lower values of λ are simultaneously associated with increased pitch-rate, less virtual camber and decreased Reynolds number. Due to the small physical dimensions of the turbine as well as the relatively low wind speed, the maximum Reynolds numbers:

$$Re_{\max} = (\lambda + 1) U_\infty c / \nu \tag{13}$$

at peak power vary between 1.6×10^5 and 2.2×10^5, for $\varepsilon = 0.6$ $(\sigma = 1.2)$ and $\varepsilon = 0.4$ $(\sigma = 0.8)$ respectively. It is well known that at these Reynolds numbers airfoils perform relatively poorly [29]. Considering the large increases in $C_{L,\max}$ and C_L / C_D, it is expected that higher Reynolds number experiments $(Re > 10^6)$ will produce higher C_P.

The profound effect of the strut attachment point is particularly intriguing. When x_c / c is further aft, the effect of virtual camber increases, and this can be best understood as if the leading-edge "droops". For example, moving x_c / c from 0.25 to 0.5 increases the leading-edge droop angle by approximately 5°. As an analogy, on many aircraft wings, a "droop-nose" or leading-edge flap is used to increase $C_{L,\max}$ and α_s for take-off and landing. This concept was extended to variable-droop leading-edges on rotorcraft blades, for the purpose of ameliorating the negative effects of dynamic stall [29],[30]. For example, for an airfoil pitching to $\alpha_{\max} = 25°$, a variable leading-edge droop of 13° eliminated the DSV and thereby significantly reduced lift hysteresis, as well as the drag rise and pitching moments. The kinematic analysis presented above shows that a similar mechanism is at play here.

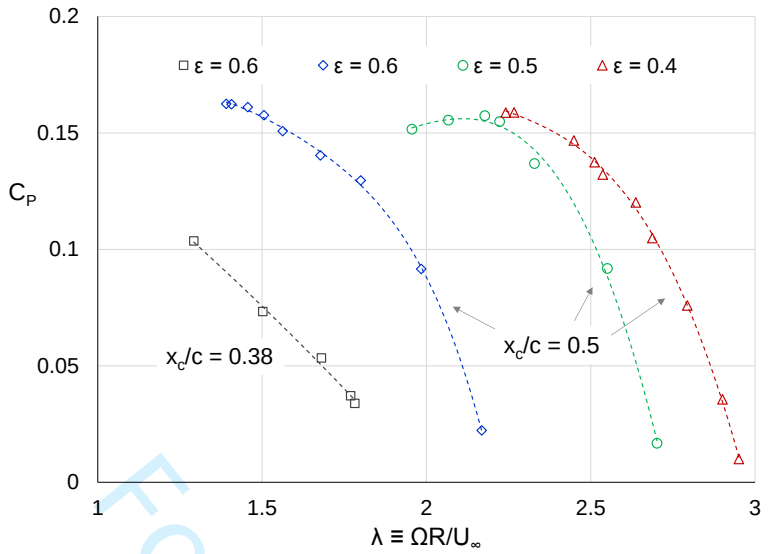

Fig. 6 Model wind turbine performance characteristics for different values of x_c / c and ε.

Another interesting difference between the present turbine performance curves and those of other turbines is the abrupt power loss when the turbine is loaded near peak power. Typically, high solidity machines have a long tail that extends well below $\lambda = 1$. This means that the advancing blades stall, while the retreating blades are being driven by drag. As the blades stall more deeply, the performance drops further leading to the appearance of a tail. There are two possible reasons for the observed difference. One is the method used to load the turbine (hysteresis brake) that is different from other investigations that employ generators [11], [31]. More likely, however, is that because the large ε turbine is being driven to peak power by dynamic stall, additional loading causes the DSV to form and shed at lower azimuthal angles. Simultaneously, the opposite blade is too far advanced into the third quadrant to produce sufficient drag for net positive torque. Thus, the different mechanism of power generation results in different qualitative performance characteristics. It is possible that a three-bladed, large ε would not exhibit the performance drop due to large drag forces imposed on the retreating blades.

Flow visualization experiments conducted with tufts attached conventionally, i.e. pointing downstream, did not produce positive results because the centrifugal forces acting on the tufts exceeded the fluid forces producing flow separation. In order to render them more sensitive to the flow, they were subsequently attached laterally, pointing vertically downward, as described in section III.A. Visualization images for $\varepsilon = 0.6$ with increasing power corresponding to $\lambda = 2$, 1.7 and 1.5 are shown in Fig. 7 for azimuthal angles between 95° and 135°. For $\lambda = 2$,

corresponding to $C_P \approx 8\%$, the tufts do not indicate flow separation for all of the azimuthal angles recorded. Although this may appear surprising because $\alpha_{max} \approx 30°$, it should be noted that the leading-edge droops by 22° and hence dynamic stall is avoided. With higher loading of the turbine, at $\lambda = 1.7$, tufts indicate incipient leading-edge separation at $\theta = 125°$, and we associate this with the formation of the DSV. Although the nominal $\alpha_{max} \approx 39°$ is large, the leading-edge has a virtual droop of 14° and the nominal $\hat{q}_{rel} = 0.35$. As the azimuth increases to $\theta = 135°$, the tufts begin to point upstream thus indicating more advanced formation of the DSV. By loading the turbine further to attain the maximum power coefficient, $C_P \approx 16\%$ at $\lambda = 1.5$ incipient leading-edge reverse flow can already be seen at $\theta = 110°$. As the blade advances further around the azimuth to $\theta = 125°$ and 135°, the reverse flow region increases and this is associated with further growth of the DSV. Note, however, that the aft tufts remain virtually unchanged and hence we can conclude that the DSV has not yet shed from the blades. When considering the flow visualization of Fig. 7 together with the power coefficient curves in Fig. 6, it becomes evident that the DSV is an integral, and indeed vital, feature associated with peak power performance. Indeed, when dynamic stall is completely absent, at $\lambda = 2$, the turbine power is relatively low. In contrast, when the DSV forms on the blade during the operation cycle, the turbine attains peak power.

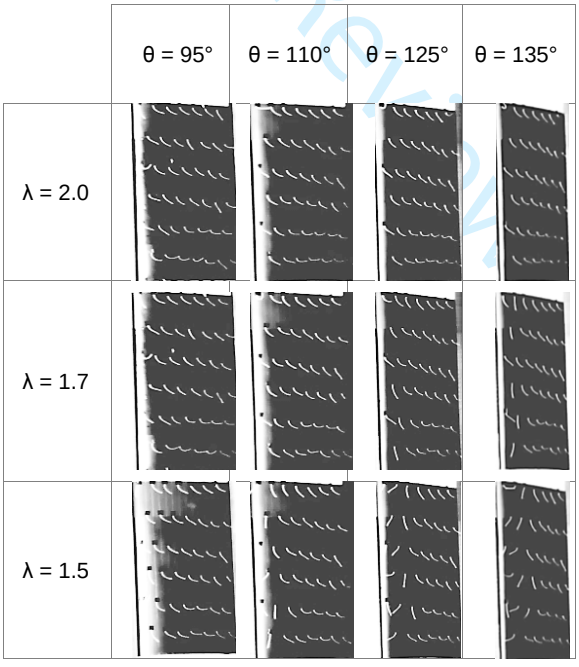

Fig. 7 Tuft grid on the wind turbine blade, inboard, with the leading-edge on the left side.

IV. Conclusions

In this paper, the concept of wind energy generation by dynamic stall was explained, the associated atypical aerodynamics were described and a model turbine was used for the purposes of demonstration. The analysis shows that these machines operate at low blade-speed/wind speed ratios and hence the blades experience large changes in angle-of-attack, associated with dynamic stall, and large dynamic pressure variations, that are phase-shifted by approximately 90°. The underlying hypothesis was that positive dynamic stall effects, associated with the generation of a dynamic stall vortex (DSV), drive the turbine when the relative dynamic pressure is high, while negative effects associated with shedding of the DSV transpire when the dynamic pressure is low and thus their effect is mitigated. The analysis also showed that the blades experience virtual camber effects and favorable pressure gradients, where the former produces a virtual leading-edge droop that reduces the leading-edge angles of attack.

Experiments demonstrated relatively low power coefficients of 16% that were virtually independent of ε between 0.4 and 0.6. It was determined, however, that the turbine strut connection point plays a critical role, where a shift forward of 25% chord from the 50% chord position, resulted in a total loss of turbine power. Another feature of the machine was an abrupt power loss when an additional load was applied at peak power. Flow visualization appeared to confirm our hypothesis that dynamic stall is the mechanism by which the turbine attains maximum power. This is an unexplored design space where conventional techniques are of little use. At this point, we have no alternative to empiricism and dimensional analysis to design machines for maximum power operation. High-fidelity CFD could also be employed to gain a deeper understanding of the physics.

In the quest to obtain greater power coefficients, a system must be designed to facilitate further aft strut attachment and blade offset angles. Different blade profiles and higher Reynolds numbers can also be expected to produce further increases in the power coefficient.

Acknowledgments

This research was supported, in part, by the Nancy and Stephen Grand Technion Energy Program and the Israeli Ministry of Energy. TDT acknowledges the research council (OZR) of the Vrije Universiteit Brussel, which supported his sabbatical leave at the Technion – Israel Institute of Technology.

References

[1] Bhutta, M.M.A., Hayat, N., Farooq, A.U., Ali, Z., Jamil, Sh.R, Hussain, Z., "Vertical axis wind turbine – A review of various configurations and design techniques," *Renewable and Sustainable Energy Reviews*, Vol. 6, Issue 4, 2012, pp. 1926-1939. doi.org/10.1016/j.rser.2011.12.004.

[2] Griffith, D.T., Paquette, J., Barone, M., Goupee, A., Fowler, M., Bull, D., Owens, B., "A Study of Rotor and Platform Design Trade-offs for Large-scale Floating Vertical Axis Wind Turbines," *Journal of Physics*: Conference Series 753, 2016, 102003, doi:10.1088/1742-6596/753/10/102003.

[3] Marten, D., Lennie, M., Pechlivanoglou, G., Paschereit, C.O., Bianchini, A., Ferrara, G., Ferrari, L., "Benchmark of a Novel Aero-Elastic Simulation Code for Small Scale VAWT Analysis," *J. Eng. Gas Turbines Power*, Vol. 141, No. 4, 2019, 041014 (13 pages).

[4] Lee, K.Y., Tsao, S.H., Tzeng, C.W. and Lin, H.J., "Influence of the vertical wind and wind direction on the power output of a small vertical-axis wind turbine installed on the rooftop of a building," *Applied Energy*, Vol. 209, No. 2018, pp. 383-391.

[5] Paraschivoiu, I., "Wind turbine design: with emphasis on Darrieus concept," Polytechnique Internationale Presse, Montreal, 2002.

[6] Ghasemian, M. and Nejat, A., "Aero-acoustics prediction of a vertical axis wind turbine using Large Eddy Simulation and acoustic analogy," *Energy*, Vol. 88, 2015, pp. 711-717.

[7] Thelander, C.G., Smallwood, K.S. and Rugge, L., "Bird risk behaviors and fatalities at the Altamont pass wind resource area," NREL/SR-500-33829, December 2003.

[8] Dominy, R.G., Lunt, P., Bickerdyke, A. and Dominy, J., "Self-starting capability of a Darrieus turbine," Proc. Inst. Mech. Eng. Part A J. Power Energy, vol. 221, no. 1, 2007, pp. 111-120.

[9] McCroskey, W. J., "Unsteady Airfoils", *Annual Review of Fluid Mechanics*, Vol. 14, pp. 285-311, 1982.

[10] Migliore, P.G., Wolfe, W.P. and Fanucci, J.B., "Flow Curvature Effects on Darrieus Turbine Blade Aerodynamics," *AIAA Journal of Energy*, Vol. 4, No. 2, 1980, pp. 49-55.

[11] Fiedler, A.J. and Tullis, S., "Blade Offset and Pitch Effects on a High Solidity Vertical Axis Wind Turbine," *Wind Engineering*, Vol. 33, No. 3, 2009, pp. 237-246.

[12] Rezaeiha, A., Kalkman, I. and Blocken, B., "Effect of pitch angle on power performance and aerodynamics of a vertical axis wind turbine, *Applied Energy*, Vol. 197, 2017, pp. 132-150. doi.org/10.1016/j.apenergy.2017.03.128.

[13] Paraschivoiu, I., "Double-Multiple Streamtube Model for Studying Vertical-Axis Wind Turbines," *AIAA Journal of Propulsion*, Vol. 4, No. 4, 1987, pp. 370-377.

[14] Ferreira, C.S. van Kuik, G., van Bussel, G. and Scarano, F., "Visualization by PIV of dynamic stall on a vertical axis wind turbine" Experiments in Fluids, Vol. 46, 2009, pp. 97-108.

[15] Carr, L. W., "Progress in the analysis and prediction of dynamic stall" *AIAA Journal of Aircraft*, Vol. 25, No. 1, 1988, pp. 6-17.

[16] Kirke, B.K. and Lazauskas, L., "Enhancing the Performance of Vertical Axis Wind Turbine Using a Simple Variable Pitch System," *Wind Engineering*, Vol. 15, No. 4, 1991, pp. 187-195.

[17] Zhu, H., Hao, W., Li, C., Ding, Q. and Wu, B., "A critical study on passive flow control techniques for straight-bladed vertical axis wind turbine," *Energy*, Vol. 165, 2018, pp. 12-25.

[18] Greenblatt, D., Schulman, M. and Ben-Harav, A., "Vertical axis wind turbine performance enhancement using plasma actuators," *Renewable Energy*, Vol. 37, 2012, pp. 345-354.

[19] Greenblatt, D., Ben-Harav, A. and Mueller-Vahl, H., "Dynamic stall control on a vertical-axis wind turbine using plasma actuators," *AIAA Journal*, Vol. 52, No. 2, 2014, pp. 456-462, DOI: 10.2514/1.J052776.

[20] Ben-Harav, A. and Greenblatt, D., "Feed-forward dynamic stall control on a vertical axis wind turbine," *Wind Energy*, Vol. 19, Issue 1, 2016, Pages 3-16. DOI: 10.1002/we.1814.

[21] Greenblatt D. and Lautman, R., "Inboard/outboard plasma actuation on a vertical-axis wind turbine" *Renewable Energy*, Vol. 83, 2015, pp. 1147-1156.

[22] Greenblatt, D. and Wygnanski, I., "Dynamic stall control by periodic excitation. Part 1: NACA 0015 Parametric Study," *AIAA Journal of Aircraft*, Vol. 38, No. 3, 2001, pp. 430-438.

[23] Greenblatt, D., "Active control of leading-edge dynamic stall," *International Journal of Flow Control*, Vol. 2, No. 1, 2010, pp. 21-38.

[24] Mueller-Vahl, H., Strangfeld, C., Nayeri, C.N., Paschereit, C.O and Greenblatt, D., "Control of thick airfoil deep dynamic stall using steady blowing," *AIAA Journal*, Vol. 53, No. 2, 2015, pp. 277-295.

[25] Buchner, A.-J., Soria, J., Honnery, D. and Smits, A.J., "Dynamic stall in vertical axis wind turbines: scaling and topological considerations," Journal of Fluid Mechanics, Vol. 841, 2018, pp. 746-766. doi:10.1017/jfm.2018.112.

[26] Greenblatt, D., "Unsteady low-speed wind tunnels," *AIAA Journal*, Vol. 54, No. 6, June 2016, pp. 1817-1830.

[27] Bell, J.H. and Mehta, R.D., "Contraction design for small low-speed wind tunnels," Department of Aeronautics and Astronautics, 1988.

[28] Li, Q., Maeda, T., Kamada, Y., Murata, J., Shimizu, K., Ogasawara, T., Nakai, A. and Kasuya, T., "Effect of solidity on aerodynamic forces around straight-bladed vertical axis wind turbine by wind tunnel experiments (depending on number of blades)," Renewable Energy, No. 96, 2016, pp. 92-939.

[29] McMasters, J. H. and Henderson, M. L., "Low-speed single-element airfoil synthesis," The Science and Technology of Low Speed and Motorless Flight, Pt. 1, 1979, pp. 1-31.

[30] Yung, H.Y., Lee, S., McAlister, K.W., Tung, C. and Wang, C.M., "Dynamic stall control for advanced rotorcraft application," *AIAA Journal*, Vol. 33, No. 2, 1995, pp. 289-295.

[31] Vergaerde, A., De Troyer, T., Carbó Molina, A., and Runacres, M.C., "Design, manufacturing and validation of a vertical-axis wind turbine setup for wind tunnel tests," *Journal of Wind Engineering and Industrial Aerodynamics*, Vol. 193, 103949, 2019, pp. 1-12.